Organic & Biomolecular Chemistry

PAPER

View Article Online
View Journal



Cite this: DOI: 10.1039/c6ob02574a

# The evaluation of 5-amino- and 5-hydroxyuracil derivatives as potential quadruplex-forming agents†

Gábor Paragi,[a,c] Zoltán Kupihár,[b] Gábor Endre,[b] Célia Fonseca Guerra*[a] and Lajos Kovács*[b]

Received 23rd November 2016,
Accepted 19th December 2016

DOI: 10.1039/c6ob02574a

www.rsc.org/obc

5-Substituted uracils ($NH_2$ or OH groups in position 5) have been examined theoretically and experimentally as potential building blocks in quadruplex structures. Our high level Density Functional Theory (DFT) calculations showed that the tetramer formation and stacking energies for 5-substituted uracils are similar to the energies of purine-based xanthine (X) or guanine (G) structures. As tetrads of 5-substituted uracils cover almost exactly the same area as purine tetrads, mixed tetrads or quadruplex structures based on X or G and 5-substituted uracil motifs are possible. According to the calculations, 5-hydroxyuracil-based structures are the best candidates for experimental implementation which was corroborated by the existence of higher complexes in the mass spectra of 1-benzyl-5-hydroxyuracil. These pyrimidine-based molecules can be used as efficient building blocks in different applications including aptamers, biosensors or – taking into account the larger cavity in the central region of 5-hydroxyuracil structures – as an artificial ion channel.

## Introduction

Beyond the well-known canonical adenine–thymine (A : T) and guanine–cytosine (G : C) base pairs in the right-handed double helix of B-DNA, there are a plethora of other possibilities, resulting in a large number of polymorphic variants. Polyguanosyl-quadruplex nucleic acids (GQs) are probably the most studied non-canonical DNA structures. A typical G-quadruplex consists of at least two guanine G-tetrads (or tetramers), most frequently connected by loops of one or more nucleotides and feature various topologies.[1] The stability of the structure is based on different components like stacking of the tetrads, cation coordination ($K^+$, $Na^+$, $NH_4^+$), hydrogen bonding or hydrophobic effects.[2–4] The cations are located either in the central cavity of the G-tetrad or in the spaces between the stacking tetrads.

Earlier we have proved that G can be replaced by model 3-alkylxanthine derivatives (X) in tetrads/octads and the resulting cation-complexed tetrads and octads are comparable with the corresponding guanine derivatives in terms of interaction energies (for canonical numbering of purine and pyrimidine rings *cf.* Fig. 1).[5] Furthermore, 3-alkylxanthines undergo self-assembly at a solid–liquid interface forming comb-like 2D structures[6] and in a bi-component system consisting of melamine and 3-octadecylxanthines, porous quasi-2D networks ensued.[7]

Other mimics of DNA bases can occur *via* oxidative damage by exposure to both endogenous and exogenous reactive oxygen species (ROS), which has been held responsible for a variety of diseases (cancer, rheumatoid arthritis, and DNA damage related to aging).[8] The most abundant base-pair substitution mutation due to oxidative damage in DNA is the G : C to A : T transition. 5-Hydroxyuracil (ho$^5$U, aka isobarbituric acid), produced by the oxidative deamination of cytosine, has been established as the major chemical precursor for this transition.[8–10] The RNA analogue, 5-hydroxyuridine has been synthesized[11] and later isolated from yeast as a modified minor RNA nucleoside.[12] 5-Hydroxy-2′-deoxyuridine (ho$^5$dUrd) has been a subject of a number of computational and experimental investigations. ho$^5$dUrd exists as a 5-hydroxy enol tautomer forming an intramolecular hydrogen bond with the carbonyl group in position 4 as evidenced by UV, X-ray data and computational studies.[8,13–15] It forms base pairs with all

[a]Department of Theoretical Chemistry and Amsterdam Center for Multiscale Modeling, Vrije Universiteit Amsterdam (VU), De Boelelaan 1083, 1081 HV Amsterdam, The Netherlands. E-mail: c.fonsecaguerra@vu.nl
[b]Department of Medicinal Chemistry, University of Szeged, Dóm tér 8, 6720 Szeged, Hungary. E-mail: kovacs.lajos@med.u-szeged.hu
[c]MTA-SZTE Supramolecular and Nanostructured Materials Research Group, University of Szeged, Dóm tér 8, 6720 Szeged, Hungary

†Electronic supplementary information (ESI) available: Computational details, $^1$H, $^{13}$C NMR and mass spectra. See DOI: 10.1039/c6ob02574a

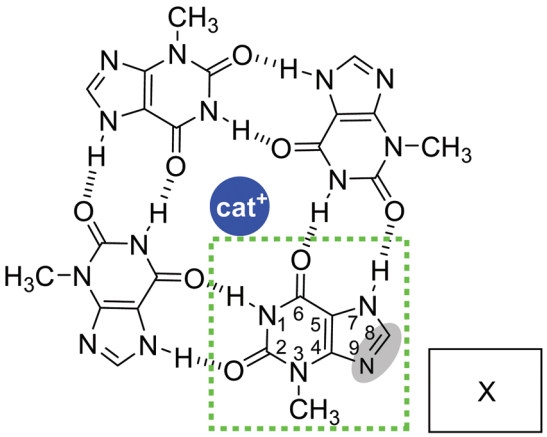


(a) 3-methylxanthine tetramer

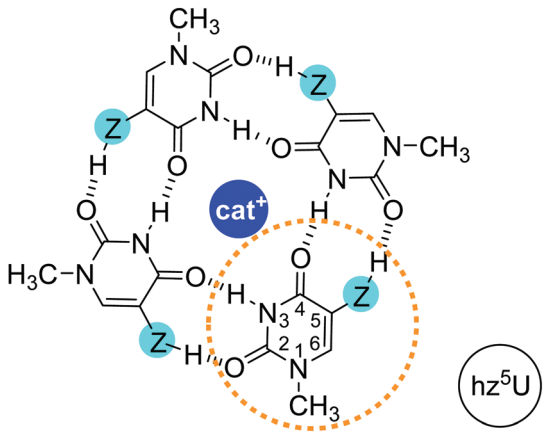


(b) 5-substituted 1-methyluracil tetramer

**Fig. 1** The hydrogen-bound tetrameric structures of 3-methylxanthine (X) [panel (a), the monomer is in dashed bold rectangle] and the result of the truncation (area shaded in grey); tetrameric assemblies of 5-substituted 1-methyluracils ($hz^5U$) [panel (b), the monomer is in dashed bold circle, where ZH = $NH_2$ or OH]. The hydrogen bonds connecting the tetrameric structures are represented by hashed lines, the abbreviation "$cat^+$" may represent cations. Schematic representations of X and $hz^5U$, along with their canonical numbering, are outlined at the right-bottom part of the structures.

natural nucleobases, from which the most stable one is with G and the least stable one is with C.[8,16–18] The replacement of base C with $ho^5U$ in the G : C base pair decreases the interaction energies of this base pair.[19] $ho^5dUrd$ is prone to further oxidative transformations.[20,21]

5-Aminouridine and its 2′-deoxy counterpart, and their $N^5$-acyl and $N^5$-alkyl derivatives (glycosylated and unglycosylated) are known to possess a wide range of biological effects, including antibacterial,[22,23] antiviral,[24] antifungal,[25] antiproliferative[26] and enzyme inhibitory activities.[27–30] 5-Amino-2′-deoxyuridine is used for high-resolution footprinting of protein–DNA complexes.[31] 5-Aminouracil PNA derivatives have been employed in redox-sensitive probes[32] and in base-pairing studies.[33] It is of particular interest that 5-amino-2′-deoxyuridine ($n^5dUrd$) is a weak replacement base for thymidine in dA : dT base pairs.[34] $n^5dUrd$, when placed in the central strand of the DNA triple helix, recognizes all four bases A, G, C, and T in the third strand, with a selectivity based on the orientation (parallel/antiparallel) of the third strand.[35–38] Only very recently Galeone *et al.* demonstrated experimentally the existence of a quadruplex structure in guanine-rich oligonucleotides containing a single 5-aminouracil tetrad[39] but a detailed theoretical analysis is still missing concerning the binding character of the new complex.

As, to the best of our knowledge, there is no detailed investigation directed towards the application of 5-substituted uracil derivatives in quadruplex research, our aim was to carefully analyze the properties of the quadruplexes containing these interesting compounds. More specifically, we were intrigued whether and how the "truncation" of the purine ring at the imidazole moiety of X (removing atoms C-8 and N-9) affects the tetrad-/quadruplex-forming potential (Fig. 1; the notation $hz^5U$ was chosen for 5-substituted uracils to harmonize with the current IUPAC nomenclature recommendations on the designation of substituents in nucleobases.[40] For the sake of simplicity, the abbreviations $hz^5U$, $n^5U$, and $ho^5U$ denote 5-substituted uracil, 5-aminouracil and 5-hydroxyuracil derivatives, respectively, regardless of the nature of the substituent in position 1). Therefore, 1,5-disubstituted uracils, containing amino or hydroxy groups in position 5 and a methyl or a benzyl group in position 1, have been considered in our present computational and experimental studies and scrutinized for their capability to form hydrogen bonds in the supposed supramolecular assemblies.

The present work will highlight the quadruplex-forming ability of single-ring based artificial nucleobases motivated by our previous 3-methylxanthine (X) study.[5] The new candidates were derived by theoretical considerations using high level DFT calculations followed by mass-spectrometric experiments demonstrating the relevance of our computational investigations.

## Results and discussion

### Derivation of the building blocks and the applied computational method

Prior to experimental work, computational simulations have been performed to forecast the self-assembling possibilities of the new molecules based on our former 3-methylxanthine (X) investigation.[5] The theoretical consideration behind selecting the candidates is demonstrated in Fig. 1, where the area shaded in grey indicates the part of xanthine that is not involved directly in the formation of a tetrad/quadruplex.

The simplest modification in which the above-mentioned part is truncated from the original xanthine led us to 5-substituted uracil ($hz^5U$) derivatives where ZH = $NH_2$ or OH (Fig. 1). The new single-ring molecules preserve the original donor/acceptor hydrogen bond pattern, therefore we expected similar

 

tetramer-forming abilities. Additionally, they can form not only pure hz$^5$U homo-tetramers but can also provide hetero-tetramers with the original xanthine molecule.

In the computational simulations a gradual protocol was followed in all cases, where the candidates were examined and compared to the original xanthine complexes in various dimer (D), tetramer (T) and octamer (O) geometries (Scheme 1). For the sake of simplicity, not all the possible combinations of the 5-substituted uracil derivatives have been considered, only the homomeric complexes and the heteromeric complexes with X units were examined computationally.

All calculations were performed with the ADF program suit at the BLYP-D3/TZ2P level of theory. The detailed description and references of the applied techniques and programs can be found in the Experimental part, as well as the basics of the energy decomposition analysis method (EDA).

### The case of 5-amino-1-methyluracil

Having completed the first step in the theoretical part, the simplest derivative of the truncated X molecule was considered as 5-amino-1-methyluracil (n$^5$U, *cf.* Fig. 1) where the broken bonds in the truncated part (*cf.* Fig. 1a, grey area) were capped by hydrogens. Although the quadruplex-forming ability of this compound was demonstrated experimentally[39] very recently as a part of a G-rich oligonucleotide chain, a high level computational analysis was completely absent which could provide a more detailed insight into the energetic character of the new tetramer structure. However, it is also necessary to be able to compare the tetramer-forming ability of the n$^5$U-based tetrad to the other (*e.g.* G- or X-based) ones without the support of four additional embracing $G_4$ layers in a heptanucleotide oligomer [d(TGGn$^5$UGGT)]$_4$ which was not investigated in the mentioned study.[39] Moreover, the reference nucleosides (thymidine and 5-bromo-2′-deoxyuridine) used in that study contained methyl and bromo substituents in position 5 which seem not relevant because these groups cannot form hydrogen bonds. Beside that fact, it was also not investigated how these electron donating and withdrawing groups (methyl and bromo, respectively) can affect the lactam–lactim tautomeric equilibrium in the pyrimidine ring which can highly affect the hydrogen bond pattern.

Thus, in our examinations, first we investigated the n$^5$U derivative computationally and compared the results to the X complexes as our reference point. We have considered all possible dimer geometries obtained from tetramers and optimized them. The minimized structures, as well as their interaction energies are presented in Fig. 2.

It is obvious from Fig. 2 that the new molecule has a considerably weaker interaction with another similar molecule (D4 in Fig. 2) and the optimum dimer geometries are also less planar compared to the original $X_2$ dimer (D1 in Fig. 2). Assuming that there is no other effect beyond the neighboring n$^5$U pair interactions, the (n$^5$U)$_4$ unit was expected to be a less stable tetramer complex and the original X-based one would be the most stable one. Indeed, comparing the interaction energies of (n$^5$U)$_4$ and $X_4$ tetramers, the new structure showed almost 25 kcal mol$^{-1}$ weaker interaction energy (−49.0 kcal mol$^{-1}$ and −73.6 kcal mol$^{-1}$, respectively) than the latter one. As the tetramer-forming ability of the (n$^5$U)$_4$ molecule is worse than that of $X_4$ the formation of an (n$^5$U)$_4$ tetrad without embracing $G_4$ layers is less feasible compared to $X_4$.

However, the results raised the question, why has n$^5$U such a different tetrameric interaction energy while it still has the same hydrogen bond pattern as X? First, it is important to notice in Fig. 2 that the interaction energy is always weaker

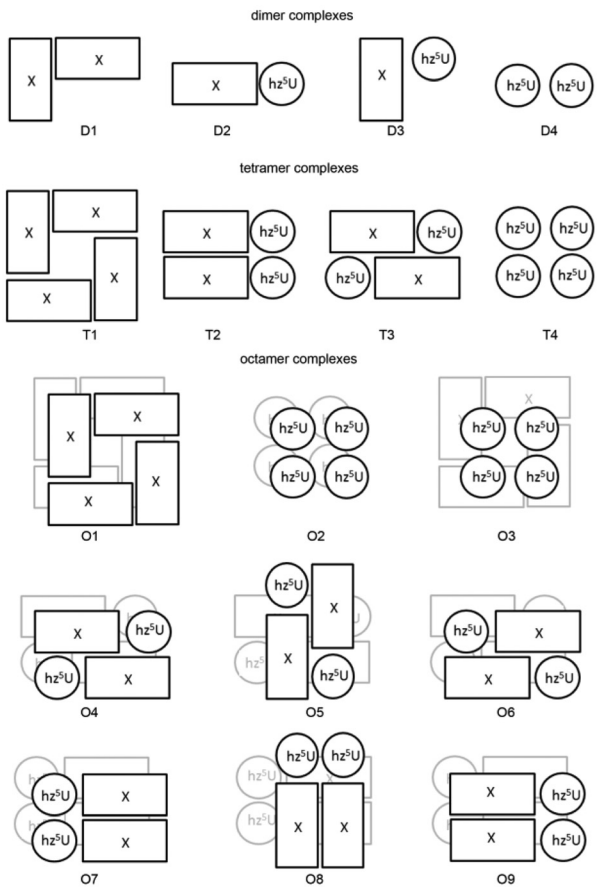


**Scheme 1** Schematic summary of the computationally investigated complexes in the present study. For simplicity, hereafter in tables and figures we will refer to the abbreviations D1–D4, T1–T4, O1–O9 introduced here.

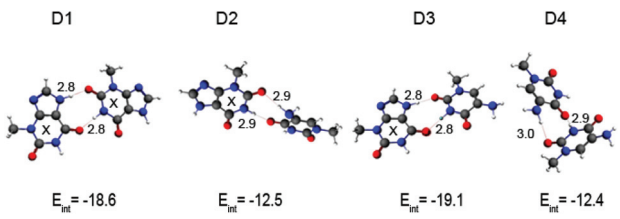


**Fig. 2** Optimum hydrogen bonds with heteroatom distances (in Å) and the interaction energies (in kcal mol$^{-1}$) of the X and n$^5$U complexes D1–D4. See also Scheme 1 for the schematic representation of the dimers. Xanthine molecules are designated with X.

when the amino group is involved in the hydrogen bonds (see Fig. 2, D2 and D4). In Table 1 we present the results of energy decomposition analysis (EDA) regarding the possible dimers and the two homo-tetramer calculations. In the dimer cases we did not apply any symmetrical restraint but for tetramers the planar restraint was used to mimic a possible $G_4$ environment or the presence of a surface. This planar restraint causes less than 1 kcal mol$^{-1}$ energy difference between the optimum in $C_{4h}$ or $C_4$ symmetry for both systems.

Previous analyses[41–45] showed that hydrogen bonds between nucleobases or derivatives thereof have a substantial covalent character as it can be seen from the significant orbital interaction component ($\Delta E_{oi}$) in the EDA. Table 1 shows clearly that in our systems the term $\Delta E_{oi}$ contributes around 35% of the attractive interactions which is in the same order of magnitude as the electrostatic component providing the remaining attraction together with the small dispersion term. This significant orbital interaction physically manifests in a charge transfer between an unoccupied $\sigma_{N-H}^*$ orbital of the proton-donor fragment and the lone pair on nitrogen or oxygen of the proton-acceptor constituent. In a clear σ–π separation (planar symmetry) the interacting orbitals are usually the $\sigma_{LUMO}$ and $\sigma_{HOMO}$ orbitals of the two monomers, and the strength of the orbital interaction is proportional to the overlapping integral and inversely proportional to the orbital energy difference between the electron donor and acceptor orbitals (see *e.g.* ref. 46).

The frontier orbitals, which significantly take part in the formation of hydrogen bonds, are presented in Fig. 3 for all three molecules examined in the present study. Considering the electron donation part of the bond formation, we found that the $\sigma_{HOMO}$ and the $\sigma_{HOMO-1}$ are the most important orbitals. For the n$^5$U molecule the free optimization does not support perfect σ–π separation due to the pyramidalization of the amino group but when planar restraints were applied, the interacting electron-donor orbitals were also the $\sigma_{HOMO}$ and the $\sigma_{HOMO-1}$ ones. Comparing the corresponding $\sigma_{HOMO}$ and $\sigma_{HOMO-1}$ orbitals of X and n$^5$U monomers, they were found to be very similar regarding the orbital energies or distributions. Hence, these orbitals cannot induce any larger changes in the interaction energies *via* the orbital interaction term. Considering the electron-acceptor orbitals in the hydrogen bonds, which are the $\sigma_{LUMO}$ and $\sigma_{LUMO+1}$ in the original X case, the corresponding $\sigma_{LUMO}$ has a completely different distribution at the amino group (*cf.* Fig. 3). More precisely, the $\sigma_{LUMO}$ is localized mainly between the methyl and the amino groups, and according to the orbital distribution, the $\sigma_{LUMO+1}$ and $\sigma_{LUMO+2}$ orbitals can play the same role in the n$^5$U molecule as the $\sigma_{LUMO}$ and $\sigma_{LUMO+1}$ orbitals in the original X one. However, this fact means a shift in the orbital energies which enlarge the denominator in the orbital energy interaction, as we described hereinabove. Thus, the orbital interaction is weakening and consequently, the total interaction as well. Taking into account that the distributions of the $\sigma_{HOMO}$ and $\sigma_{HOMO-1}$ orbitals are very similar for both molecules, in the next step we aimed at changing the $\sigma_{LUMO}$ part of the molecule.

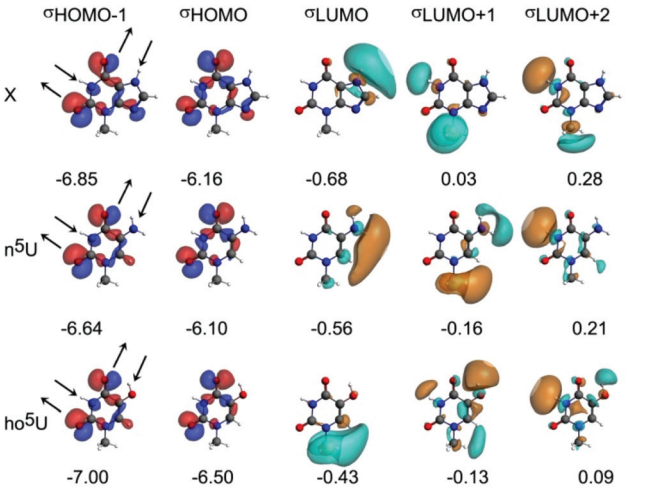


**Fig. 3** Frontier σ orbitals with orbital energy (in eV) regarding the quadruplex formation. Geometries are taken from optimized monomers with planar restraint and the arrows in the first column show the direction of the electron donation in the hydrogen bonds.

According to Fig. 3, the main problem regarding the weaker interaction of the new molecule is that the capping hydrogen in the amino group of the truncated X molecule localizes the $\sigma_{LUMO}$ as well as the $\sigma_{LUMO+1}$ to the non-bonding part of the n$^5$U molecule. Moreover, the analogue of the $\sigma_{LUMO+1}$ of X is also shifted with one level higher in n$^5$U which is also weakening the orbital interaction energy. Concerning the EDA, it means smaller absolute value for each term but the change in the attractive terms ($\Delta V_{elstat}$, $\Delta E_{oi}$) altogether are larger than in the repulsive one ($\Delta E_{Pauli}$). Thus, we aimed at redirecting the LUMO orbital distribution to the interacting region in a new molecule. The simplest solution to provide a more directed electron-acceptor LUMO orbital is the substitution of the amino group by a hydroxy group in position 5. According to our expectation this modification (n$^5$U → ho$^5$U) can strengthen the total interaction energy *via* a better orbital interaction term. Furthermore, the complex of the new molecule can be more planar because of the flexibility of the hydroxy group which is beneficial in the tetramer formation.

**Table 1** EDA energy terms (in kcal mol$^{-1}$) of X and n$^5$U dimer complexes optimized without constraint (nosym case) and the planarly restricted ($C_{4h}$ case) homotetramers of the two units

| | X$_2$ (D1)[a] | (n$^5$U)$_2$ (D4) | X–n$^5$U (D3) | X–n$^5$U (D2) | X$_4$ (T1) | (n$^5$U)$_4$ (T4) |
|---|---|---|---|---|---|---|
| $\Delta E_{int}$ | −18.6 | −12.5 | −19.1 | −12.4 | −73.0 | −51.0 |
| $\Delta E_{Pauli}$ | 29.6 | 20.7 | 30.6 | 21.5 | 121.9 | 85.4 |
| $\Delta V_{elstat}$ | −26.0 | −18.2 | −26.7 | −18.2 | −102.7 | −74.9 |
| $\Delta E_{oi}$ | −18.0 | −11.0 | −18.7 | −11.3 | −74.6 | −46.4 |
| $\Delta E_{disp}$ | −4.1 | −3.9 | −4.2 | −4.4 | −17.6 | −15.1 |

[a] For the definition of geometries D1–D4, T1 and T4 see Scheme 1.

### The case of 5-hydroxy-1-methyluracil

As we pointed out in the previous section, the truncation of the non-interacting part of the X molecule led to a weaker tetrameric structure. Focusing onto the important frontier orbitals in the interaction, the analysis allowed us to identify 5-hydroxy-1-methyluracil ($ho^5U$) as a pyrimidine derivative with promising tetramer forming ability. By inspecting the frontier orbitals in the $ho^5U$ monomer molecule (bottom row in Fig. 3), it is clear that the amino to hydroxy substitution did not alter the $\sigma_{HOMO}$ and $\sigma_{HOMO-1}$ distributions, it only shifted the energies by 0.4 eV. Considering the $\sigma_{LUMO}$, $\sigma_{LUMO+1}$ and $\sigma_{LUMO+2}$ orbitals, there are larger changes. Although the substitution cannot heal the problem of the $\sigma_{LUMO}$ distribution, in the $\sigma_{LUMO+1}$ case there are significant changes regarding the orbital distribution. Namely, one can see a noteworthy orbital lobe around the OH group, which points toward the requested direction. Very similar orbital redistribution appeared in the $\sigma_{LUMO+2}$ case which renders the $ho^5U$ molecule a promising candidate.

Following the hierarchy of the computational investigations, first we examined those dimer interactions which take part in the formation of the tetramers. In Fig. 4 we summarized them similarly to Fig. 2, where all the relevant homo- and hetero-dimer connections are considered. One of the striking features of these calculations is the nice planarity of the optimized structures. This is the simple consequence of the fact that there are no pyramidalization effects in the $ho^5U$ complexes which would enforce the non-planar geometry of the fragments. This can help the formation of tetramer structures, as well as the incorporation into other quadruplex structures (*e.g.* $G_4$ or $X_4$). The other important result is that the interaction energies significantly improved, and the D3 mixed complex in Fig. 4 has the largest interaction energy out of all dimer interactions considered in this paper.

In Table 2 the EDA terms of all three homo-dimers [$X_2$, $(n^5U)_2$, $(ho^5U)_2$] have been compared. We found that always the $X_2$ dimer has the largest value in absolute sense but the $(ho^5U)_2$ energy terms are much closer to the $X_2$ results than to the $(n^5U)_2$ ones. We would like to highlight that these orbital interaction energy values corroborate our expectation regarding the better frontier orbital interactions in the $X_2$ and $(ho^5U)_2$ cases with respect to the dimer $(n^5U)_2$.

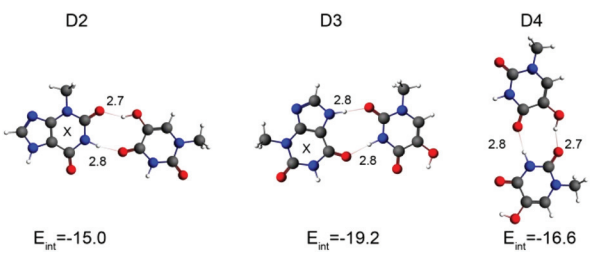


**Fig. 4** Optimized dimer geometries of $ho^5U$ complexes with optimum distances (in Å) and their interaction energies (in kcal $mol^{-1}$). Xanthine molecules are designated with X.

**Table 2** Total interaction energies ($\Delta E_{int}$) and the EDA terms (in kcal $mol^{-1}$) for all three homodimers

| | $X_2$ (D1)[a] | $(n^5U)_2$ (D4) | $(ho^5U)_2$ (D4) |
|---|---|---|---|
| $\Delta E_{int}$ | −18.6 | −12.5 | −16.6 |
| $\Delta E_{Pauli}$ | 29.6 | 20.7 | 28.4 |
| $\Delta V_{elstat}$ | −26.0 | −18.2 | −24.4 |
| $\Delta E_{oi}$ | −18.0 | −11.0 | −16.7 |
| $\Delta E_{disp}$ | −4.1 | −3.9 | −3.9 |

[a] For the definition of geometries D1 and D4 see Scheme 1.

After the investigation of the tetramer-forming ability of the $ho^5U$ candidate, we calculated all the tetrads which are mentioned in Scheme 1. In Table 3 the interaction energies as well as the corresponding EDA terms have been summarized.

It is obvious from Table 3 that both mixed tetrameric structures provide approximately 10% larger interaction energy than the pure $(ho^5U)_4$ tetramer. This is in line with our experiments where the formation of the mixed tetramers is more common. The clear σ–π separation (planar restraint) reveals that the σ electronic system has a principal role in the formation of the tetramers, as it yields the vast majority of the orbital interaction term. In summary we can say that the interaction character of these tetrameric structures could be predicted accurately from the previous molecular orbital analysis based on monomer and dimer complexes.

Finally, we would like to highlight certain geometrical aspects of the optimized tetramers. In Fig. 5 the optimized geometries of the planar $(ho^5U)_4$ and $X_4$ structures are shown, and the diagonal distances between two oxygen atoms (connected to the C(6) atom), as well as the distance between the methyl groups of two adjacent units are presented. Taking into account the four-fold symmetry of the systems, it is obvious that the two complexes cover almost exactly the same area. Considering the connection points to the sugar phosphate backbone (represented by the methyl groups), Fig. 5 exhibits clearly that the distances between the backbones are almost exactly the same. Thus, it can be expected that the new derivatives can be easily incorporated into quadruplex structures based on X or G tetramers. This is the consequence of the similar methyl-group distances, due to the fact that when real

**Table 3** Total interaction energies ($\Delta E_{int}$) with respect to the monomers and the results of the EDA (in kcal $mol^{-1}$) for $ho^5U$- and X-based tetramers. All geometries were optimized in planar symmetry

| Tetramers (geometries)[a] | $(ho^5U)_2 + X_2$ (T2 geom.) | $(ho^5U)_2 + X_2$ (T3 geom.) | $(ho^5U)_4$ (T4 geom.) |
|---|---|---|---|
| $\Delta E_{int}$ | −66.0 | −66.2 | −60.8 |
| $\Delta E_{Pauli}$ | 113.4 | 114.8 | 105.1 |
| $\Delta V_{elstat}$ | −95.8 | −96.5 | −89.3 |
| $\Delta E_{oi}$ | −67.5 | −68.3 | −61.6 |
| $\Delta E_{oi}(\sigma)$ | −60.7 | −61.4 | −55.7 |
| $\Delta E_{oi}(\pi)$ | −6.8 | −6.9 | −5.9 |
| $\Delta E_{disp}$ | −16.1 | −16.2 | −14.9 |

[a] For the definition of geometries T2, T3 and T4 see Scheme 1.

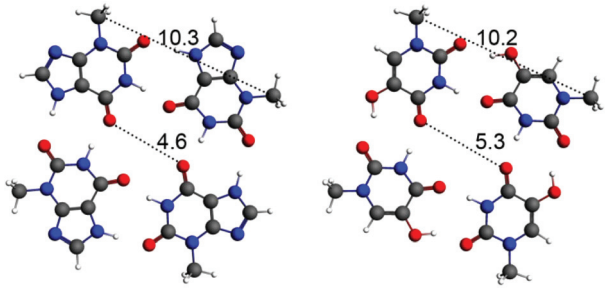


Fig. 5 Optimized planar tetramer structures of $X_4$ (left) and $(ho^5U)_4$ (right) complexes with selected distances (in Å).

sugar-phosphate spines are connected in that position, this backbone does not have to be distorted to adopt the optimum geometry. The cluster formation of $ho^5U$ (see mass spectrometric evidence later) convincingly supports our computational results.

The second important consequence of the present tetramer geometry is that the central cavity in the $ho^5U$ complex has some 15% (0.7 Å) larger diameter than the $X_4$ one (Fig. 5). It provides space for larger cations in the center region, as well as it can alter the ion mobility character of the central channel, which could be important for the design of new quadruplex-based artificial ion channels.[47–51]

### Octamer structures and ion binding

The final step in the theoretical part was the investigation of the stacking of tetrads. It is important to note that the presence of a cation ($Na^+$, $K^+$, $NH_4^+$) in the central channel of quadruplexes is essential as it stabilizes the quadruplex formation. Thus, beyond the stacking possibilities, the ion-binding abilities were also examined. The simplest stacked geometry is the octamer structure with two tetramer layers where the tetramers are positioned above each other with or without the cation in the central cavity of the complex. Obviously, the stacking interaction plays an important role in the formation of an octamer by stabilizing the connection between adjacent layers,[52–54] but the effect of the central cation (when present) is also important. To distinguish the effect of these two interactions, we examined the "empty" octamers and the octamers with cations separately.

The stacking possibility of the new candidates was investigated in the first step in homo-octamers where all the building blocks were identical in the structure. According to Scheme 1, this is the O1 case for the original X molecule and the O2 arrangement for the $n^5U$ or $ho^5U$ derivatives, respectively. Following the geometrical optimization, we determined the interaction energies between the two layers, and the results were −53.0 kcal $mol^{-1}$, −48.4 kcal $mol^{-1}$ and −51.4 kcal $mol^{-1}$ for the $X_8$, $(n^5U)_8$ and $(ho^5U)_8$ structures, respectively. These numbers clearly illustrate that the stacking interaction is almost the same for the old and the new systems. This is in contrast to our expectation as we supposed that the purine-based octamer will have considerably larger stacking interaction. Moreover, the stacking energy between two different homo-tetramers (O3 in Scheme 1) was found to be −51.5 kcal $mol^{-1}$ for the $(ho^5U)_4 + X_4$ complex which forecasts a promising quadruplex-forming ability for the new building block in combination with purine-based quadruplex structures. This character of the $n^5U$ tetrads was experimentally proven by Galeone *et al.* in a recent paper[39] showing that the $n^5U$ bases form a tetramer structure between the guanine layers of oligonucleotide $[d(TGGn^5UGGT)]_4$.

Calculating the mixed octamer structures (*cf.* O4–O9 in Scheme 1) for the $ho^5U$ and X complexes we found that the stacking energy was always around −50 kcal $mol^{-1}$ (see Table SI-1 in the ESI†). This fact indicates that *almost any combination* of the new candidate $ho^5U$ with the X molecule is conceivable which is very useful in the design of new aptamers or bio-sensors.

The last part in the computational investigation of the new molecules was the cation binding analysis of the systems. At the end of the previous section we highlighted the importance of the size of the cavity in the center of the tetramer structure. It is well known that cations can bind to this region in quadruplex structures and ion coordination can greatly contribute to the formation of quadruplex structures.[52–54] The optimized structures of $X_8$ and $(ho^5U)_8$ quadruplexes with ammonium cation are presented in Fig. 6 (top and side views). We would like to note that during the optimization we did not require planar symmetry for the tetramer layers, however, the side views indicate that the layers kept the planar geometry quite well. The interaction energies between the $NH_4^+$ ion and the octamer structures were found to be −105.6 kcal $mol^{-1}$ and −104.1 kcal $mol^{-1}$ for the clusters $[X_8 + NH_4]^+$ and $[(ho^5U)_8 + NH_4]^+$ respectively. Similar small differences were calculated in the presence of $Na^+$, namely −126.3 kcal $mol^{-1}$ and −125.0 kcal $mol^{-1}$ interaction energies for the clusters $[X_8 + Na]^+$ and $[(ho^5U)_8 + Na]^+$, respectively, while there was almost no difference in the case of the $K^+$ ion ($E_{int}[X_8 + K]^+$ = −104.2 kcal $mol^{-1}$ and $E_{int}[(ho^5U)_8 + K]^+$ = −104.8 kcal $mol^{-1}$). These values are in line with our previous results.[4]

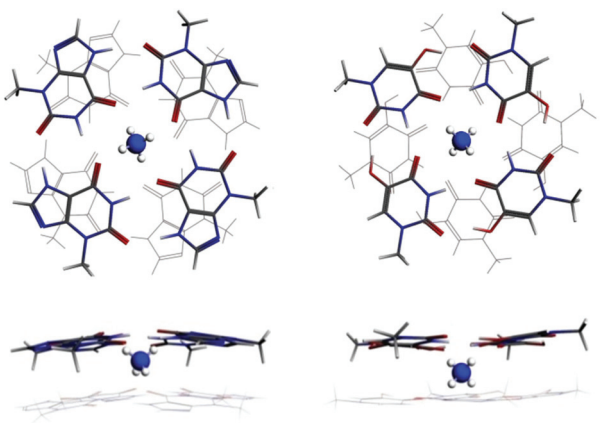

Fig. 6 Optimized $X_8$ (left) and $(ho^5U)_8$ octamers (right) with the $NH_4^+$ cation in the central position.

Nevertheless, it would be interesting to calculate the ion mobility of larger quadruplex structures, but this investigation is beyond the scope of the present work.

An additional difference between the original and the new quadruplex systems was found in relation to the optimal relative twist of adjacent layers. Explicitly, the twist angle of the two layers was always larger in the $(ho^5U)_8$ case than in the $X_8$ complex, independently from the presence or absence of a cation. However, we would like to emphasize the shallow character of the minima regarding the twist angle. For example, rotating the two layers (without relaxation) with +5 and −5 degrees in the $(ho^5U)_8$ case provides only 0.8 and 1.2 kcal mol$^{-1}$ change in the total energy, respectively. Although in the $NH_4^+$ case the orientation of the hydrogens can strongly influence the relative orientation of the layers, in the less directed $[X_8 + K]^+$ complex the twist angle of the optimized structure was 21.8° while the same angle was 44.1° in the $[(ho^5U)_8 + K]^+$ system. This latter value means that an almost perfect staggered conformation is present in this complex. According to ref. 55 the twist angle was found larger than 40° for G-quadruplexes only in a special quadruplex backbone topology. But taking into account the shallow character of the energy minimum regarding the twist angle, the backbone can easily bridge the difference between the two optima.

### ESI-MS analyses of cluster formation of 5-amino- and 5-hydroxyuracil derivatives

In our previous work the experimental method which indicated the existence of tetrameric structures in the gas phase was the ESI-MS technique.[5] Therefore, 1-methyl- and 1-benzyluracil derivatives have been investigated with the ESI-MS technique to observe the presence of the tetrameric complexes. The benzyl derivative of 5-hydroxyuracil was chosen for the sake of simplicity as methylation of the starting 5-bromouracil gave poor yields and mixtures that were difficult to purify.[56]

The ESI mass spectrum of 5-amino-1-methyluracil did not reveal the presence of higher-order structures, only simple adducts ($[M + cat]^+$, cat = H, $NH_4$, Na) could be observed. To ascertain whether 5-amino-1-methyluracil exhibits the propensity of replacing 3-methylxanthine in tetrads/octads, 5-amino-1-methyluracil has been mixed with 3-methylxanthine and the mass spectrum of this mixture was recorded. Indeed, low-intensity mixed dimers and trimers containing one 5-amino-1-methyluracil and ammonium ion (omnipresent in mass spectrometers) could be detected even without added salts but no other clusters could be observed (Fig. 7). Purposefully added ammonium salts did not alter this situation.

The mass spectra of 1-benzyl-5-hydroxyuracil ($ho^5U$, $M$ = 218) in the absence of added salts showed protonated monomeric ($[M + H]^+$) and dimeric ($[2M + H]^+$) species but no higher-order clusters could be observed. Upon the addition of ammonium salts into aqueous solutions of methanol or 1,1,1,3,3,3-hexafluoroisopropanol (HFIP) a series of low-intensity ammonium adducts with 2, 3, 4, 5, 8 and 12 uracil moieties appeared (Fig. 8). We have noted that increasing the concentration of HFIP enhanced the signal-to-noise ratio and/or stabilized the clusters.

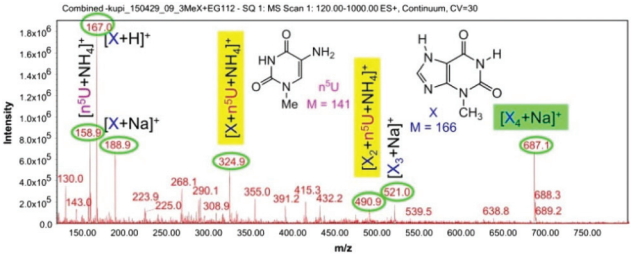


Fig. 7 Mixed ESI-MS spectrum of 5-amino-1-methyluracil ($n^5U$; $M$ = 141) and 3-methylxanthine (X; $M$ = 166) without added salt.

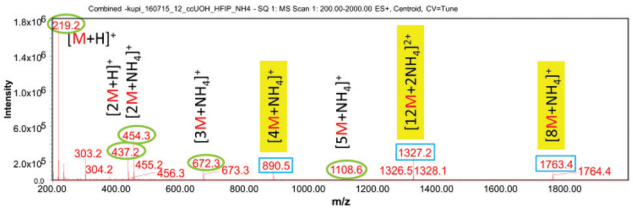


Fig. 8 ESI-MS spectrum of 1-benzyl-5-hydroxyuracil ($ho^5U$, $M$ = 218) in the presence of ammonium hydrogen carbonate in HFIP.

The separation of overlapping isobaric singly and doubly charged species ($[6M + NH_4]^+$ and $[12M + 2NH_4]^{2+}$, $m/z$ = 1327 for both entities) could be achieved using electrospray ionization field asymmetric waveform ion mobility mass spectrometry combined with mass spectrometry (ESI-FAIMS-MS).[57] This is a special MS technique requiring sophisticated instrumentation. Fortunately, in our case this separation could be simply attained by analyzing the isotopic distribution of the high resolution mass spectrum (Fig. 9) which unequivocally confirmed that the peaks around $m/z$ = 1327 originate from the doubly charged dodecameric species $[12M + 2NH_4]^{2+}$ which is very likely a triple-layered quadruplex structure (multiple charged sodiated complexes of 3-methylxanthine (X) with

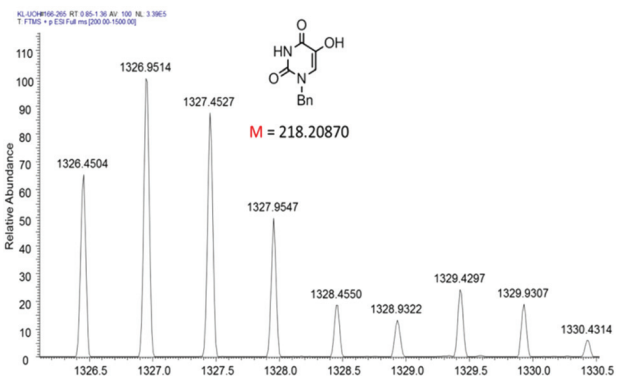


Fig. 9 Isotopic distribution of the peak $[12M + 2NH_4]^{2+}$ of 1-benzyl-5-hydroxyuracil ($ho^5U$, $M$ = 218.20870) (high resolution mass spectrum).

up to 32 units, *e.g.* $[(X_4)_8 + 6Na - 3H]^{3+}$, have been previously reported[57]).

The experimental finding that in the mass spectra of 1-benzyl-5-hydroxyuracil, tetra-, octa- and dodecameric species appeared *only* upon addition of ammonium salts invalidates the assumption that eventual stacking interactions exerted by the benzyl side groups would significantly contribute to the stability of the above clusters. Instead, hydrogen bonding, governed by ion coordination is the principal stabilizing factor in cluster formation of ho$^5$U derivatives. The quantum mechanical calculations of Marek *et al.*[52–54] underscore that stacking between nucleobases plays a subordinate role in stabilizing ion-bound clusters: stacking provides 10% of the formation energies *in vacuo* for guanine octamers $[(G_4)_2 + cat]^+$ (cat = Na, K), 12–14% for xanthine octamers $[(X_4)_2 + cat]^+$ (cat = Na, K), 12–14% for guanine dodecamers $[(G_4)_3 + 2cat]^{2+}$ (cat = Na, K) and 19–21% for xanthine dodecamers $[(X_4)_3 + 2cat]^{2+}$ (cat = Na, K) as deduced from the energy decomposition analyses[53] (in water the stacking term is slightly higher, especially for xanthine).[52,54]

A series of adduct-forming salts ($NH_4^+$, $Na^+$, $K^+$, $Ca^{2+}$, $Sr^{2+}$ and $Ba^{2+}$ cations) have also been tested with ho$^5$U and various adducts have been detected (*e.g.* $[8M + cat]^{2+}$, cat = Ca, Sr) but $NH_4^+$ formed the most intensive complexes, *e.g.* $[4M + NH_4]^+$ (ESI, Fig. SI-9†). The ESI-MS spectrum of a mixture containing 1-benzyl-5-hydroxyuracil and 3-methylxanthine has also been recorded and the replacement of one or two 3-methylxanthine moieties by 1-benzyl-5-hydroxyuracil could be observed in tetrads and octads (Fig. 10). The experimentally found X : ho$^5$U = 3 : 1 and 7 : 1 stoichiometries in these clusters previously have not been calculated but as it was pointed out earlier, almost any combination of ho$^5$U with the X moiety is conceivable owing to the very similar tetrad-/octad-forming character of X and ho$^5$U bases.

These observations are in good correlation with the computational predictions, *viz.*, (1) 5-aminouracil derivatives form weak clusters, while (2) 5-hydroxyuracil-containing clusters are comparable in stability with those formed from 3-methylxanthine.

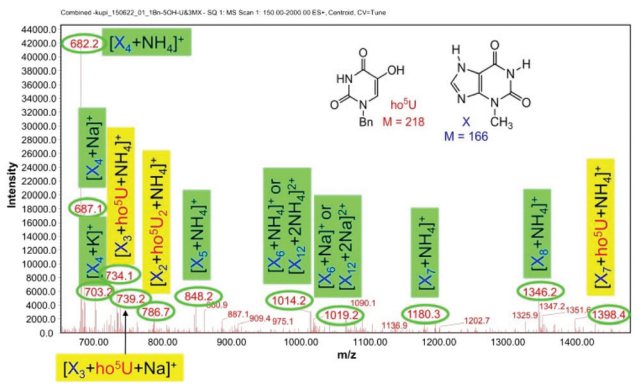


**Fig. 10** Mixed ESI-MS spectrum of 1-benzyl-5-hydroxyuracil (ho$^5$U, *M* = 218) and 3-methylxanthine (X, *M* = 166) without added salt. The exact composition of peaks at *m*/*z* 1014 and 1019 (whether they represent the clusters $[6X + NH_4]^+$ or $[12X + 2NH_4]^{2+}$) and $[6X + Na]^+$ or $[12X + 2Na]^{2+}$, respectively) was not investigated in detail.

# Experimental

## Computational methods

All calculations were performed with the Amsterdam Density Functional (ADF) program[58–68] and QUILD[69,70] using dispersion-corrected relativistic density functional theory at the BLYP-D3/TZ2P[71–75] level for geometry optimizations and energies. The overall bond energy $\Delta E_{bond}$ is made up of two major components:

$$\Delta E_{bond} = \Delta E_{prep} + \Delta E_{int} \quad (1)$$

In this formula, the preparation energy $\Delta E_{prep}$ is the amount of energy required to deform the separate bases from their equilibrium structure to the geometry that they acquire in the tetrad. The interaction energy $\Delta E_{int}$ corresponds to the actual energy change when the prepared bases are combined to form the tetrad.

The interaction energy is examined in the framework of the Kohn–Sham MO model using a quantitative energy decomposition analysis (EDA) into electrostatic interactions, Pauli repulsive orbital interactions, and attractive orbital interactions, to which a term $\Delta E_{disp}$ is added to account for the dispersion interactions:[76]

$$\Delta E_{int} = \Delta V_{elstat} + \Delta E_{Pauli} + \Delta E_{oi} + \Delta E_{disp} \quad (2)$$

The term $\Delta V_{elstat}$ corresponds to the classical electrostatic interactions between the unperturbed charge distributions of the prepared (*i.e.* deformed) bases and is usually attractive. The Pauli repulsion $\Delta E_{Pauli}$ comprises the destabilizing interactions between occupied orbitals and is responsible for any steric repulsion. The orbital interaction $\Delta E_{oi}$ accounts for charge transfer (*i.e.*, donor–acceptor interactions between occupied orbitals on one moiety and unoccupied orbitals on the other, including the HOMO–LUMO interactions) and polarization (empty–occupied orbital mixing on one fragment due to the presence of another fragment).

The orbital interaction energy can be further decomposed into the contributions from each irreducible representation $\Gamma$ of the interacting system (eqn (3)) using the extended transition state (ETS) scheme developed by Ziegler and Rauk.[77–79] In planar systems, the symmetry partitioning allows us to distinguish σ and π interactions:

$$\Delta E_{oi} = \Delta E_{oi}(\sigma) + \Delta E_{oi}(\pi) \quad (3)$$

## Synthesis

Unless otherwise noted, solvents and reagents were reagent grade from commercial suppliers and used without further purification. 5-Amino-1-methyluracil[80,81] has been purchased from ZereneX Molecular (UK). 5-Bromouracil has been synthesized from uracil according to a published method.[82] All

 

moisture-sensitive reactions were performed under an argon atmosphere using oven-dried glassware. Reactions were monitored by TLC on Kieselgel 60 $F_{254}$ plates (Merck) with detection by UV. Flash column chromatography was carried out using silica gel (particle size 40–63 μm). Melting points (uncorrected): Electrothermal IA 8103 apparatus. Elementary analyses: Perkin-Elmer CHN analyzer model 2400. $^1$H and $^{13}$C NMR spectra were recorded in DMSO-$d_6$ using a Bruker Avance DRX 500 instrument and assignments are based on *J*-modulated spin-echo experiments. ESI-MS analyses were performed on a Waters Acquity SQD mass spectrometer (positive ionization mode) and the high resolution spectra were recorded on a Thermo Fisher Scientific Q Exactive™ Plus Hybrid Quadrupole-Orbitrap™ Mass Spectrometer (positive ionization mode).

**Benzylation of 5-bromouracil.** 5-Bromouracil (2.00 g, 10.47 mmol) was dissolved in anhydrous DMF (40 mL) under sonication. Anhydrous $K_2CO_3$ was added (1.446 g, 10.46 mmol, 1.0 equiv.) and the heterogeneous solution was stirred at room temperature for 15 min. The obtained potassium salt was treated dropwise with benzyl bromide (1.306 mL, 10.996 mmol, 1.05 equiv.) and the reaction mixture was stirred at room temperature for 22 h. The heterogeneous solution was acidified with acetic acid, evaporated *in vacuo* and co-evaporated with $CH_3CN$ (2×). The residue was dissolved in water (50 mL) and extracted with EtOAc (3 × 75 mL). The combined organic layers were dried ($MgSO_4$), filtered and evaporated *in vacuo*. The crude product was purified by column chromatography using the solvent system 3–5 v/v% isopropanol in toluene to give 1-benzyl-5-bromouracil (1.211 g, 41.1%) and 1,3-dibenzyl-5-bromouracil (1.312 g, 33.8%).

**1-Benzyl-5-bromouracil.** An analytical sample has been obtained from the previously purified title compound by recrystallisation from isopropanol. Mp.: 209.7–210.6 °C. ESI-MS (*m*/*z*): 281.0 (100, $[(^{79}Br)M + H]^+$), 283.0 (95, $[(^{81}Br)M + H]^+$). $^1$H NMR (*δ*, ppm): 4.84 (s, 2 H, $CH_2$), 7.05–7.48 (m, 5 H, arom.), 8.30 (s, 1 H, H-6), 11.81 (br. s, deuterable, 1 H, NH). $^{13}$C NMR (*δ*, ppm): 50.8 ($CH_2$), 95.2 (C-5), 127.5, 127.8, 128.7 (arom. CHs), 136.5 (C-1′), 145.2 (C-6), 150.4 (C-2), 159.7 (C-4). Elemental analysis calcd (%) for $C_{11}H_9BrN_2O_2$ (281.105) C, 47.00; H, 3.23; Br, 28.42; N, 9.97, found C, 47.18; H, 3.40; Br, 28.63; N, 9.81.

**1,3-Dibenzyl-5-bromouracil.** An analytical sample has been obtained from the previously purified title compound by recrystallisation from isopropanol. Mp.: 123.0–125.5 °C (dec.). ESI-MS (*m*/*z*): 371.1 (100, $[(^{79}Br)M + H]^+$), 373.1 (95, $[(^{81}Br)M + H]^+$). $^1$H NMR (*δ*, ppm): 4.96 (s, 2 H, $CH_2$), 5.02 (s, 2 H, $CH_2$), 7.14–7.38 (m, 10 H, arom.), 8.50 (s, 1 H, H-6). $^{13}$C NMR (*δ*, ppm): 45.1 ($CH_2$), 52.1 ($CH_2$), 94.5 (C-5), 127.3, 127.6, 127.7, 127.9, 128.4, 128.7 (arom. CHs), 136.3 (C-1′), 136.6 (C-1′), 144.2 (C-6), 150.6 (C-2), 158.8 (C-4). Elemental analysis calcd (%) for $C_{18}H_{15}BrN_2O_2$ (371.228) C, 58.24; H, 4.07; Br, 21.52; N, 7.55, found C, 58.03; H, 4.26; Br, 21.68; N, 7.71.

**1-Benzyl-5-hydroxyuracil.** 1-Benzyl-5-bromouracil has been hydrolysed according to a published method.[83] The crude product was purified by column chromatography using the solvent system 1 : 9 : 90 v/v% acetic acid/isopropanol/toluene to afford the title compound.

Mp.: 226–227 °C (sinters from 210 °C). ESI-MS (*m*/*z*): 219.1 (100, $[M + H]^+$), 236.0 (10, $[M + NH_4]^+$), 437.1 (25, $[2M + H]^+$), 454.1 (31, $[2M + NH_4]^+$), 672.2 (33, $[3M + NH_4]^+$), 890.3 (5, $[4M + NH_4]^+$), 1326.7 (3, $[12M + 2NH_4]^{2+}$), 1763.4 (4, $[8M + NH_4]^+$). $^1$H NMR (*δ*, ppm): 4.78 (s, 2 H, $CH_2$), 7.19 (s, 1 H, H-6), 7.22–7.36 (m, 5 H, arom.), 8.66 (br. s, deuterable, 1 H, OH), 11.46 (br. s, deuterable, 1 H, NH). $^{13}$C NMR (*δ*, ppm): 49.9 ($CH_2$), 124.6 (C-6), 127.5, 127.6, 128.7 (arom. CHs), 132.5 (C-5), 137.1 (C-1′), 149.6 (C-2), 160.9 (C-4). Elemental analysis calcd (%) for $C_{11}H_{10}N_2O_3$ (218.209) C, 60.55; H, 4.62; N, 12.84, found C, 60.34; H, 4.78; N, 12.71.

### ESI-MS data of aggregates

The samples were prepared in the following way: a saturated aqueous solution of solute, containing 100 mM solution of $NH_4HCO_3$ (pH = 8) and methanol saturated with $NH_4HCO_3$ were mixed in a 1 : 99 ratio and the resulting diluted solutions were used directly for the experiments. In some experiments 1-benzyl-5-hydroxyuracil has been dissolved in water or in water containing 1,1,1,3,3,3-hexafluoroisopropanol (HFIP), in a 1 : 1 (v/v) ratio, or in neat HFIP. Analogously, for the experiments with other complex-forming salts, aqueous solutions of NaCl, KCl, $Ca(NO_3)_2$, $Sr(NO_3)_2$ and $Ba(NO_3)_2$ have been used with an initial concentration of 100 mM each.

## Conclusions

In the present work, we have investigated theoretically and experimentally the quadruplex-forming ability of 5-substituted uracil derivatives as analogues of 3-substituted xanthine derivatives with a truncated imidazole ring. We showed computationally that the recently suggested 5-aminouracil ($n^5$U) is not the most optimal building block for self-assembled tetramers or quadruplex structures. Based on our careful quantum chemical orbital analysis and EDA method we recommend a new unit, expected to be more suitable: 5-hydroxyuracil ($ho^5$U). The self-assembly of the new candidate was corroborated by ESI-MS experiments as well and we found that the new entity provides encouraging cation-bound complexes either alone or in combination with the 3-methylxanthine (X) unit.

Comparing the geometrical features of the $ho^5$U-based and X-based complexes, we encountered that the central cavity is larger in the former case. This can open the way for further investigations related to cation binding and cation mobility properties along the central cavity channel. Nevertheless, our calculations underlined that the new structures can bind cations in this region as well.

Moreover, the relative positions of the backbone connection points in the $ho^5$U and X tetramers are almost the same, which indicates that the new building block can be incorporated into quadruplex structures without any difficulty. Our experimental and theoretical results convincingly demonstrated the excellent self-assembly ability of $ho^5$U. Therefore,

the inclusion of the 5-hydroxyuracil moiety into mixed tetrameric or octameric structures with 3-substituted xanthines is very promising.

## Acknowledgements

G. P. would like to thank the Marie Curie Intra European Fellowship within the 7th European Community Framework Programme for the financial support. C. F. G. acknowledges the financial support from the Netherlands Organization for Scientific Research NWO (ECHO). The authors are grateful to Mrs Brigitta Bodnár for recording the NMR spectra.

## Notes and references

1 S. Neidle and S. Balasubramanian, *Quadruplex Nucleic Acids*, The Royal Society of Chemistry, Cambridge, 2006.
2 J.-L. Mergny, A. De Cian, A. Ghelab, B. Saccà and L. Lacroix, *Nucleic Acids Res.*, 2005, **33**, 81–94.
3 E. Largy, J.-L. Mergny and V. Gabelica, in *The Alkali Metal Ions: Their Role for Life*, ed. A. Sigel, H. Sigel and O. R. K. Sigel, Springer International Publishing, Cham, 2016, pp. 203–258, DOI: 10.1007/978-3-319-21756-7_7.
4 F. Zaccaria, G. Paragi and C. Fonseca Guerra, *Phys. Chem. Chem. Phys.*, 2016, **18**, 20895–20904.
5 J. Szolomájer, G. Paragi, G. Batta, C. Fonseca Guerra, F. M. Bickelhaupt, Z. Kele, P. Pádár, Z. Kupihár and L. Kovács, *New J. Chem.*, 2011, **35**, 476–482.
6 A. Ciesielski, S. Haar, A. Bényei, G. Paragi, C. Fonseca Guerra, F. M. Bickelhaupt, S. Masiero, J. Szolomájer, P. Samorì, G. P. Spada and L. Kovács, *Langmuir*, 2013, **29**, 7283–7290.
7 A. Ciesielski, S. Haar, G. Paragi, Z. Kupihár, Z. Kele, S. Masiero, C. Fonseca Guerra, F. M. Bickelhaupt, G. P. Spada, L. Kovács and P. Samorì, *Phys. Chem. Chem. Phys.*, 2013, **15**, 12442–12446.
8 V. Thiviyanathan, A. Somasunderam, D. E. Volk, T. K. Hazra, S. Mitra and D. G. Gorenstein, *Biochem. Biophys. Res. Commun.*, 2008, **366**, 752–757.
9 J. Fujimoto, L. Tran and L. C. Sowers, *Chem. Res. Toxicol.*, 1997, **10**, 1254–1258.
10 C. J. La Francois, Y. H. Jang, T. Cagin, W. A. Goddard and L. C. Sowers, *Chem. Res. Toxicol.*, 2000, **13**, 462–470.
11 M. Roberts and D. W. Visser, *J. Am. Chem. Soc.*, 1952, **74**, 668–670.
12 A. W. Lis and W. E. Passarge, *Arch. Biochem. Biophys.*, 1966, **114**, 593–595.
13 R. C. B. Copley, L. S. Deprez, T. C. Lewis and S. L. Price, *CrystEngComm*, 2005, **7**, 421–428.
14 S. A. Barnett, A. T. Hulme, N. Issa, T. C. Lewis, L. S. Price, D. A. Tocher and S. L. Price, *New J. Chem.*, 2008, **32**, 1761–1775.
15 T. Lukmanov, S. P. Ivanov, E. M. Khamitov and S. L. Khursan, *Comput. Theor. Chem.*, 2013, **1023**, 38–45.
16 A. A. Purmal, Y. W. Kow and S. S. Wallace, *Nucleic Acids Res.*, 1994, **22**, 72–78.
17 V. Thiviyanathan, A. Somasunderam, D. E. Volk and D. G. Gorenstein, *Chem. Commun.*, 2005, 400–402.
18 D. E. Volk, V. Thiviyanathan, A. Somasunderam and D. G. Gorenstein, *Org. Biomol. Chem.*, 2006, **4**, 1741–1745.
19 Z. M. Qiu, H. J. Wang and Y. M. Xia, *Struct. Chem.*, 2010, **21**, 931–937.
20 H. Inoue, S. Koizume, T. Yamauchi, K. Murata and E. Ohtsuka, *Nucleosides Nucleotides*, 1997, **16**, 1489–1490.
21 P. Simon, D. Gasparutto, S. Gambarelli, C. Saint-Pierre, A. Favier and J. Cadet, *Nucleic Acids Res.*, 2006, **34**, 3660–3669.
22 R. E. Beltz and D. W. Visser, *J. Biol. Chem.*, 1957, **226**, 1035–1045.
23 D. W. Visser, in *Antineoplastic and Immunosuppressive Agents: Part II*, ed. A. C. Sartorelli and D. G. Johns, Springer, Berlin, Heidelberg, 1975, pp. 373–383, DOI: 10.1007/978-3-642-65806-8_17.
24 T. Y. Shen, J. F. McPherson and B. O. Linn, *J. Med. Chem.*, 1966, **9**, 366–369.
25 M. Roberts and D. W. Visser, *J. Biol. Chem.*, 1952, **194**, 695–701.
26 S. Noll, M. Kralj, L. Suman, H. Stephan and I. Piantanida, *Eur. J. Med. Chem.*, 2009, **44**, 1172–1179.
27 M. Friedland and D. W. Visser, *Biochim. Biophys. Acta*, 1961, **51**, 148–152.
28 D. A. Smith, P. Roy-Burman and D. W. Visser, *Biochim. Biophys. Acta*, 1966, **119**, 221–228.
29 A. Hampton, F. Kappler and R. R. Chawla, *J. Med. Chem.*, 1979, **22**, 621–631.
30 J. Balzarini, E. De Clercq, M. P. Mertes, D. Shugar and P. F. Torrence, *Biochem. Pharmacol.*, 1982, **31**, 3673–3682.
31 M. J. Storek, A. Suciu and G. L. Verdine, *Org. Lett.*, 2002, **4**, 3867–3869.
32 G. Gasser, M. J. Belousoff, A. M. Bond and L. Spiccia, *J. Org. Chem.*, 2006, **71**, 7565–7573.
33 G. K. Mittapalli, Y. M. Osornio, M. A. Guerrero, K. R. Reddy, R. Krishnamurthy and A. Eschenmoser, *Angew. Chem., Int. Ed.*, 2007, **46**, 2478–2484.
34 D. A. Barawkar, R. K. Kumar and K. N. Ganesh, *Tetrahedron*, 1992, **48**, 8505–8514.
35 V. S. Rana, D. A. Barawkar and K. N. Ganesh, *J. Org. Chem.*, 1996, **61**, 3578–3579.
36 V. S. Rana and K. N. Ganesh, *Org. Lett.*, 1999, **1**, 631–633.
37 V. S. Rana and K. N. Ganesh, *Nucleic Acids Res.*, 2000, **28**, 1162–1169.
38 E. Ferrer, G. Neubauer, M. Mann and R. Eritja, *J. Chem. Soc., Perkin Trans. 1*, 1997, 2051–2058.
39 V. Esposito, A. Pepe, R. Filosa, L. Mayol, A. Virgilio and A. Galeone, *Org. Biomol. Chem.*, 2016, **14**, 2938–2943.
40 IUPAC-IUB Commission on Biochemical Nomenclature (CBN), *Pure Appl. Chem.*, 1974, **40**, 277–290.
41 C. Fonseca Guerra, F. M. Bickelhaupt, J. G. Snijders and E. J. Baerends, *Chem. – Eur. J.*, 1999, **5**, 3581–3594.

 

42 C. Fonseca Guerra, F. M. Bickelhaupt and E. J. Baerends, *ChemPhysChem*, 2004, **5**, 481–487.
43 G. Paragi, E. Szájli, F. Bogár, L. Kovács, C. Fonseca Guerra and F. M. Bickelhaupt, *New J. Chem.*, 2008, **32**, 1981–1987.
44 C. Fonseca Guerra, H. Zijlstra, G. Paragi and F. M. Bickelhaupt, *Chem. – Eur. J.*, 2011, **17**, 12612–12622.
45 L. Guillaumes, S. Simon and C. Fonseca Guerra, *ChemistryOpen*, 2015, **4**, 318–327.
46 T. A. Albright, J. K. Burdett and M.-H. Whangbo, *Orbital interactions in chemistry*, Wiley, New York, 1985.
47 S. Bahmanjah, N. Zhang and J. T. Davis, *Chem. Commun.*, 2012, **48**, 4432–4434.
48 J. Novotný, P. Kulhánek and R. Marek, *J. Phys. Chem. Lett.*, 2012, **3**, 1788–1792.
49 G. W. Gokel and S. Negin, *Acc. Chem. Res.*, 2013, **46**, 2824–2833.
50 E. Marchal, S. Rastogi, A. Thompson and J. T. Davis, *Org. Biomol. Chem.*, 2014, **12**, 7515–7522.
51 J. R. Burns, A. Seifert, N. Fertig and S. Howorka, *Nat. Nanotechnol.*, 2016, **11**, 152–156.
52 S. Bazzi, J. Novotný, Y. P. Yurenko and R. Marek, *Chem. – Eur. J.*, 2015, **21**, 9414–9425.
53 Y. P. Yurenko, J. Novotný, V. Sklenář and R. Marek, *Phys. Chem. Chem. Phys.*, 2014, **16**, 2072–2084.
54 J. Novotný, Y. P. Yurenko, P. Kulhánek and R. Marek, *Phys. Chem. Chem. Phys.*, 2014, **16**, 15241–15248.
55 R. V. Reshetnikov, A. M. Kopylov and A. V. Golovin, *Acta Naturae*, 2010, **2**, 72–81.
56 I. I. Kuzmenko, V. N. Bobkov and T. V. Zvolinskaya, *Zh. Obshch. Khim.*, 1989, **59**, 1751–1755.
57 K. L. Arthur, G. A. Eiceman, J. C. Reynolds and C. S. Creaser, *J. Am. Soc. Mass Spectrom.*, 2016, **27**, 800–809.
58 E. J. Baerends, D. E. Ellis and P. Ros, *Chem. Phys.*, 1973, **2**, 41–51.
59 E. J. Baerends and P. Ros, *Chem. Phys.*, 1975, **8**, 412–418.
60 E. J. Baerends and P. Ros, *Int. J. Quantum Chem.*, 1978, **12**, 169–190.
61 J. G. Snijders, P. Vernooijs and E. J. Baerends, *At. Data Nucl. Data Tables*, 1981, **26**, 483–509.
62 P. M. Boerrigter, G. T. Velde and E. J. Baerends, *Int. J. Quantum Chem.*, 1988, **33**, 87–113.
63 L. Versluis and T. Ziegler, *J. Chem. Phys.*, 1988, **88**, 322–328.
64 G. T. Velde and E. J. Baerends, *J. Comput. Phys.*, 1992, **99**, 84–98.
65 C. Fonseca Guerra, J. G. Snijders, G. te Velde and E. J. Baerends, in *Methods and Techniques for Computational Chemistry*, ed. G. C. E. Clementi, STEF, Cagliari, 1995, pp. 305–395.
66 C. Fonseca Guerra, J. G. Snijders, G. te Velde and E. J. Baerends, *Theor. Chem. Acc.*, 1998, **99**, 391–403.
67 G. te Velde, F. M. Bickelhaupt, E. J. Baerends, C. Fonseca Guerra, S. J. A. Van Gisbergen, J. G. Snijders and T. Ziegler, *J. Comput. Chem.*, 2001, **22**, 931–967.
68 T. Z. E. J. Baerends, J. Autschbach, D. Bashford, A. Bérces, F. M. Bickelhaupt, C. Bo, P. M. Boerrigter, L. Cavallo, D. P. Chong, L. Deng, R. M. Dickson, D. E. Ellis, M. van Faassen, L. Fan, T. H. Fischer, C. Fonseca Guerra, M. Franchini, A. Ghysels, A. Giammona, S. J. A. van Gisbergen, A. W. Götz, J. A. Groeneveld, O. V. Gritsenko, M. Grüning, S. Gusarov, F. E. Harris, P. van den Hoek, C. R. Jacob, H. Jacobsen, L. Jensen, J. W. Kaminski, G. van Kessel, F. Kootstra, A. Kovalenko, M. V. Krykunov, E. van Lenthe, D. A. McCormack, A. Michalak, M. Mitoraj, S. M. Morton, J. Neugebauer, V. P. Nicu, L. Noodleman, V. P. Osinga, S. Patchkovskii, M. Pavanello, P. H. T. Philipsen, D. Post, C. C. Pye, W. Ravenek, J. I. Rodríguez, P. Ros, P. R. T. Schipper, G. Schreckenbach, J. S. Seldenthuis, M. Seth, J. G. Snijders, M. Solà, M. Swart, D. Swerhone, G. te Velde, P. Vernooijs, L. Versluis, L. Visscher, O. Visser, F. Wang, T. A. Wesolowski, E. M. van Wezenbeek, G. Wiesenekker, S. K. Wolff, T. K. Woo and A. L. Yakovlev, *ADF2013*, SCM, Theoretical Chemistry, Vrije Universiteit, Amsterdam, 2013.
69 M. Swart and F. M. Bickelhaupt, *Int. J. Quantum Chem.*, 2006, **106**, 2536–2544.
70 M. Swart and F. M. Bickelhaupt, *J. Comput. Chem.*, 2008, **29**, 724–734.
71 A. D. Becke, *Phys. Rev. A*, 1988, **38**, 3098–3100.
72 C. T. Lee, W. T. Yang and R. G. Parr, *Phys. Rev. B: Condens. Matter*, 1988, **37**, 785–789.
73 S. Grimme, *J. Comput. Chem.*, 2004, **25**, 1463–1473.
74 S. Grimme, *J. Comput. Chem.*, 2006, **27**, 1787–1799.
75 S. Grimme, J. Antony, S. Ehrlich and H. Krieg, *J. Chem. Phys.*, 2010, **132**, 154104.
76 F. M. Bickelhaupt and E. J. Baerends, *Rev. Comput. Chem.*, 2000, **15**, 1–86.
77 T. Ziegler and A. Rauk, *Theor. Chim. Acta*, 1977, **46**, 1–10.
78 T. Ziegler and A. Rauk, *Inorg. Chem.*, 1979, **18**, 1558–1565.
79 T. Ziegler and A. Rauk, *Inorg. Chem.*, 1979, **18**, 1755–1759.
80 T. C. Thurber and L. B. Townsend, *J. Heterocycl. Chem.*, 1975, **12**, 711–716.
81 P. Pecorari, G. Vampa, A. Albasini, M. Rinaldi, M. Melegari and M. P. Costi, *Farmaco*, 1988, **43**, 311–318.
82 S. Y. Wang, *J. Org. Chem.*, 1959, **24**, 11–13.
83 P. K. Basu and A. Ghosh, *J. Iran. Chem. Soc.*, 2013, **10**, 55–62.